Rod Visual Pigment Optimizes Active State to Achieve Efficient G protein Activation as Compared to Cone Visual Pigments*

Keiichi Kojima, Yasushi Imamoto, Ryo Maeda, Takahiro Yamashita, and Yoshinori Shichida[1]

Department of Biophysics, Graduate School of Science, Kyoto University, Kyoto 606-8502, Japan.

*****Running Title: *Rhodopsin exhibits efficient G protein activation*

[1]To whom correspondence should be addressed: Yoshinori Shichida, Department of Biophysics, Graduate School of Science, Kyoto University, Kyoto 606-8502, Japan, Tel.: +81-75-753-4213; Fax: +81-75-753-4210; E-mail: shichida@rh.biophys.kyoto-u.ac.jp.

Keywords; G protein coupled receptors (GPCR), Membrane proteins, Rhodopsin, Membrane bilayer, UV spectroscopy, Fluorescence spectroscopy, G protein activation efficiency

Background: Relationship between the properties of visual pigment and the photoreceptor amplification efficiency is controversial.
Results: Rhodopsin activates G protein more efficiently than cone pigments.
Conclusion: Visual pigment properties are directly related to the photoreceptor sensitivity diversification.
Significance: Amplification of cell responses is regulated by receptor molecules.

ABSTRACT

Most vertebrate retinas contain two types of photoreceptor cells, rods and cones, which show different photoresponses to mediate scotopic and photopic vision, respectively. These cells contain different types of visual pigments, rhodopsin and cone visual pigments, respectively, but little is known about the molecular properties of cone visual pigments under physiological conditions, which has made it difficult to link the molecular properties of rhodopsin and cone visual pigments with the differences in photoresponse between rods and cones. Here we prepared bovine and mouse rhodopsin (bvRh and mRh), and chicken and mouse green-sensitive cone visual pigments (cG and mG) embedded in nanodiscs and applied time-resolved fluorescence spectroscopy to compare their Gt activation efficiencies. Rhodopsin exhibited greater Gt activation efficiencies than cone visual pigments. Especially, the Gt activation efficiency of mRh was about 2.5-fold greater than that of mG at 37 °C, which is consistent with our previous electrophysiological data of knock-in mice. While the active state (Meta-II) was in equilibrium with inactive states (Meta-I and Meta-III), quantitative determination of Meta-II in the equilibrium showed that the Gt activation efficiency per Meta-II of bvRh was also greater than those of cG and mG. These results indicated that efficient Gt activation by rhodopsin, resulting from an optimized active state of rhodopsin, is one of the causes of the high amplification efficiency of rods.

Most vertebrate retinas contain two types of photoreceptor cells, rods and cones, which are responsible for scotopic and photopic vision, respectively. Rods are more sensitive to light than cones, while cones display a more rapid photoresponse and rapid adaptation than rods (1-2). Despite the striking difference in photoresponses between rods and cones, accumulated evidence indicates that both cells have a similar signal transduction cascade, suggesting that the differences in photoresponse between rods and cones could originate from differences in the molecular properties and concentrations of transduction proteins (*2-5*). Therefore, whether or not the properties of rod and cone visual pigments are directly related to the photoresponse of rods and cones has been a long-standing issue.

A visual pigment is a photoreceptor molecule that contains 11-*cis*-retinal as its chromophore. The role of a visual pigment is to absorb a photon and activate G protein (*6*). Thus, if a visual pigment efficiently absorbs a photon and efficiently activates G protein, the photosensitivity of the photoreceptor cell is

high. To elucidate the contribution of rod and cone visual pigments to the photoresponse of photoreceptor cells, we have produced knock-in mice whose rods express mouse green-sensitive cone visual pigment (mG) instead of rhodopsin (*7*). Electrophysiological assays showed that rods containing mG have amplification efficiency about one-third that of wild-type rods. Because the amplification efficiency of the transduction cascade per bleached pigment in mouse rods was about 6.8-fold higher than that in mouse cones (*8*), the electrophysiological assay results implied that about half of the difference in amplification efficiency between rods and cones is derived from the difference of visual pigments (7-8).

It has previously been reported that the Gt activation efficiencies of rhodopsin and cone visual pigments were similar to each other based on experiments performed at about 0 °C (7,9-10), although those of rhodopsin and cone visual pigments of a poikilothermic animal (carp) were recently reported to be different at 20 °C (11-12). Thus, it is likely that the difference in amplification efficiency between wild-type rods and rods containing mG is caused by temperature-dependent intrinsic properties of visual pigments such as the thermal equilibrium between active state Meta-II and its precursor Meta-I and/or the lifetime of Meta-II that may compete with the deactivation process consisting of phosphorylation by rhodopsin kinase (*7*). Regarding the latter possibility, Shi et al. reported that the response profile of mouse rods containing mouse UV cone pigment differed depending on whether rod arrestin was present or absent, although the effect of arrestin was not very strong (*13*). That finding does not, of course, rule out the possibility that the Gt activation efficiencies of rhodopsin and cone visual pigments are different at physiological temperature (37ºC) due to different temperature dependence of the Gt activation efficiency between rhodopsin and cone visual pigments.

Since the decay of the active state of cone visual pigments at 37ºC was expected to be too fast to permit measurement of Gt activation efficiency by conventional biochemical assays, we considered it desirable to prepare cone visual pigment samples whose environment would be similar to that of the photoreceptor cell membranes and which could be subjected to spectroscopic measurements with high time-resolution. For this purpose, we used nanodiscs to prepare the samples.

Nanodiscs are soluble membrane particles that consist of phospholipids and membrane scaffold protein(s) (MSPs) (14-15), into which membrane proteins such as GPCRs can be inserted (*16-18*). It has been reported that rhodopsin in nanodiscs effectively activated Gt (*19*) and was inactivated by GRK1 and visual arrestin (20-21) and that β2 adrenergic receptor in nanodiscs effectively activated Gs (*22*). These findings indicate that spectroscopic assays using nanodisc samples are an alternative to biochemical assays using native membranes or liposomes.

In this study, we prepared nanodisc samples containing bvRh, mRh, cG and mG. Cone visual pigments are phylogenetically classified into four groups, the S (SWS1), M1 (SWS2), M2 (RH2) and L (LWS)-groups (*23-25*). Among them, the M2 and L groups are phylogenetically the closest to and farthest from the rhodopsin-group (RH-group), respectively, and we therefore selected cG from the M2 group and mG from the L-group for the present analyses.

We confirmed that nanodiscs mimic the native membrane environment, and compared the Gt activation efficiencies of photoactivated bvRh, mRh, cG and mG. Then, using the ratios of Meta-II at equilibrium determined from time-resolved spectroscopic measurements, we calculated the Gt activation efficiency per Meta-II. From these results, the contribution of Gt activation efficiency to the photoresponses of rods and cones, and the mechanism giving rise to the different Gt activation efficiencies between rhodopsin and cone visual pigments, are discussed.

EXPERIMENTAL PROCEDURES

Preparation of Pigments—Bovine rod outer segments (ROS) were isolated from fresh bovine retina, as previously described (*26*). Recombinant bvRh, mRh, cG, and mG were transiently expressed in HEK293T cell lines as previously reported (*27*). The cDNAs of cG and mG were tagged by the epitope sequence of the monoclonal antibody Rho1D4 (ETSQVAPA) at the C-terminus. The transfected cells were collected by centrifugation and suspended in Buffer A (50 mM HEPES, 140 mM NaCl, pH

6.5), and 11-*cis*-retinal was added to the cell suspension to reconstitute photoactive pigments. They were solubilized with Buffer B (0.75 % CHAPS, 50 mM HEPES, 140 mM NaCl, 3 mM $MgCl_2$, pH 7.5), and adsorbed to a Rho1D4 affinity column (27-28). After the column was washed with Buffer B containing phospholipids (the mixture of 0.78mM POPC and 0.52 mM POPG, 1.3mM POPC, or the mixture of 0.78 mM DOPC and 0.52 mM POPG), the pigment was eluted by the addition of the synthetic peptide having the epitope sequence. To obtain purified bvRh in DM suspension, the transfected cells were solubilized with Buffer C (50 mM HEPES, 140 mM NaCl, 3 mM $MgCl_2$, pH 7.5) containing 1 % DM and adsorbed to a Rho1D4 affinity column. After washing with Buffer C containing 0.02 % DM, bvRh was eluted by addition of the peptide.

Preparation of Nanodiscs—MSP1E3D1 was used as the membrane scaffold protein (MSP) of nanodiscs. It was expressed in *E. coli* and purified as described previously (*14*). MSP was quantitated by absorbance at 280 nm (29910 M^{-1} cm^{-1}). MSP was mixed with phospholipids (POPC/POPG, POPC or DOPC/POPG in Buffer B) and purified recombinant pigment at the molar ratio of 750 : 10 : 1 (lipids : MSP : pigment) to prepare nanodiscs containing monomeric pigment (20,29). The mixture was dialyzed against Buffer D (140 mM Tris/HCl, 50 mM NaCl, 5 mM EDTA, pH 7.4) at 4 °C to reconstitute the nanodiscs by removing detergent. The aggregates and liposomes were removed from the mixture using a Superdex 200 column. The collected fractions containing nanodiscs were further purified by Rho1D4 affinity column chromatography in Buffer C to remove the empty nanodiscs.

Spectroscopic Measurements—Absorption spectra of the samples were recorded using a UV-visible spectrophotometer (Shimadzu UV-2450, UV-2400). The temperature of the samples was kept at 0 °C by using a cell holder equipped with a circulation system for the temperature-controlled water. Time-resolved absorption spectra were recorded using a high-speed CCD spectrophotometer (C10000 System, Hamamatsu Photonics) (27,30). This spectrophotometer continuously acquires full spectra (2048 channels) with a wavelength resolution of about 0.5 nm at time intervals of 0.2 ms. For spectroscopic measurements, ROS and nanodiscs were suspended in Buffer C. The sample temperature was maintained by using a cell holder equipped with a Peltier device. The samples were irradiated with an Nd:YAG laser at 532 nm (Minilite-II, Continuum) 100 ms after the measurements were started.

Analysis of Time-resolved Spectroscopic Data—The spectral changes were analyzed by singular value decomposition (SVD) and global fitting methods by using the software Igor Pro (WaveMetrics Inc.) (27,31). The difference spectra after photo-excitation were arranged in matrix *A*. Its columns and rows correspond to absorbance vs wavelength and absorbance vs time after photo-excitation, respectively. The SVD calculation decomposed *A* into a product of a left singular matrix *U*, a diagonal matrix containing singular values *S*, and a transpose of a right singular matrix *V* as follows:

$$A = U \times S \times V^{\mathrm{T}} \quad \text{(Eq.1)}$$

We determined the number of columns considered in the following estimation (*n*) from the number of significant singular values and basis spectra in matrices *U* and *V*.

$$A = U \times S \times V^{T} \approx U_n \times S_n \times V_n^{\mathrm{T}} \quad \text{(Eq. 2)}$$

where U_n and V_n^{T} contain *n* columns and S_n contains *n* singular values. Assuming that all the transitions from one intermediate to another are first-order reactions, V_n^T was fitted with the sum of exponential functions as follows:

$$V_n^{\mathrm{T}} = C \times (\exp(-k_1 t_i), \exp(-k_2 t_i), \cdots \exp(-k_{n-1} t_i), 1)^{\mathrm{T}} \quad \text{(Eq. 3)}$$

Matrix *C* contains amplification factors of exponential function ($\exp(-k_j t_i)$), and t_i is the time after photon absorption at which the *i*th spectrum was measured. From Eqs. 1-3, the matrix *A* can be expressed as follows:

$$A \approx U_n \times S_n \times C \times (\exp(-k_1 t_i), \exp(-k_2 t_i), \cdots \exp(-k_{n-1} t_i), 1)^{\mathrm{T}} \quad \text{(Eq. 4)}$$

The *j*th column of $U_n \times S_n \times C$ is the b-spectrum that represents the kinetic

component with rate constant k_j. The *n*th column of the $U_n \times S_n \times C$ is the b0 spectrum that corresponds to the constant spectrum at infinite time. In this paper, the opposite-signed b-spectra are shown except for b0.

Preparation of Bovine Rod Gt—Bovine rod Gt was purified from bovine retina as previously described (*32*). The concentration of Gt was estimated by the Bradford assay. Purified Gt was stored in Buffer C.

Gt Activation Assay and Estimation of Initial Velocities—Gt activation was measured using fluorescence assays. Fluorescence changes of intrinsic Trp of Gt were monitored using a laboratory-constructed photon counting system with some modifications (*30*). Briefly, the excitation beam was generated using a Jasco J-600 spectropolarimeter. Fluorescence was detected using a photon counting head (H7360-01, Hamamatsu Photonics) connected to the controller unit (C8855, Hamamatsu Photonics). Fluorescence greater than 310 nm was collected using an optical filter (U-360) in front of the photon counting head. Counting duration was 100 ms. The pigments were irradiated with a yellow flash generated by a combination of a short-ark xenon flash lamp (SA-200F, Nissin Electronic) and a Y-52 filter.

Gt activation efficiency was evaluated using the initial velocities as previously described (*30*). For bvRh and mRh, the initial slopes of the fluorescence increase in the presence and absence of Gt were calculated, and then the initial velocity of fluorescence increase due to Gt activation ($V_0^{F(\mathrm{Gt}\rightarrow\mathrm{Gt}*)}$) was obtained by subtracting the latter from the former.

On the other hand, while Meta-II of cG and mG decay into opsin during the Gt activation (Scheme 1), $V_0^{F(\mathrm{Gt}\rightarrow\mathrm{Gt}*)}$ were analyzed based on the Michaelis-Menten kinetics as follows (*30*).

In Scheme 1, concentration changes of Gt, Meta-II, Meta-II·Gt and opsin are expressed as follows:

$$\frac{d[\mathrm{Gt}^*]}{dt} = k_{\mathrm{cat}} \times [\mathrm{Meta\text{-}II \cdot Gt}] \quad \text{(Eq. 5)}$$

$$\frac{d[\mathrm{Meta\text{-}II}]}{dt} = -(k_{\mathrm{r}} + k_{\mathrm{a}}[\mathrm{Gt}])[\mathrm{Meta\text{-}II}] + (k_{\mathrm{d}} + k_{\mathrm{cat}})[\mathrm{Meta\text{-}II \cdot Gt}] \quad \text{(Eq. 6)}$$

$$\frac{d[\mathrm{Meta\text{-}II \cdot Gt}]}{dt} = k_{\mathrm{a}}[\mathrm{Gt}][\mathrm{Meta\text{-}II}] - (k_{\mathrm{d}} + k_{\mathrm{cat}})[\mathrm{Meta\text{-}II \cdot Gt}] \quad \text{(Eq. 7)}$$

$$\frac{d[\mathrm{Opsin}]}{dt} = k_{\mathrm{r}}[\mathrm{Meta\text{-}II}] \quad \text{(Eq. 8)}$$

As the total amount of Meta-II, Meta-II·Gt, and opsin is constant:

$$[\mathrm{Meta\text{-}II}]_{t=0}^{\mathrm{total}} = [\mathrm{Meta\text{-}II}] + [\mathrm{Meta\text{-}II \cdot Gt}] + [\mathrm{Opsin}] \quad \text{(Eq. 9)}$$

In the present experimental conditions, Meta-II of cone visual pigments rapidly decays before the depletion of Gt. Assuming that the concentration of Gt is constant, these differential equations (Eqs. 5-9) can be solved as follows:

$$[Meta\text{-}II \cdot Gt] = [Meta\text{-}II]_{t=0}^{total} \times \frac{k_a[Gt]}{(-k_r^{'}+k_r^{''})}\left(exp\left(-k_r^{'}t\right) - exp\left(-k_r^{''}t\right)\right) \quad \text{(Eq. 10)}$$

$$[\mathrm{Opsin}] = [\mathrm{Meta\text{-}II}]_{t=0}^{\mathrm{total}} \times \left\{\frac{(k_{\mathrm{r}}''-k_{\mathrm{r}})}{-k_{\mathrm{r}}'+k_{\mathrm{r}}''}(1-\exp(-k_{\mathrm{r}}'t)) - \frac{(k_{\mathrm{r}}'-k_{\mathrm{r}})}{-k_{\mathrm{r}}'+k_{\mathrm{r}}''}(1-\exp(-k_r''t))\right\} \quad \text{(Eq. 11)}$$

where $k_{\mathrm{r}}^{'}$ and $k_{\mathrm{r}}^{''}$ are the apparent rate constants expressed as follows:

$$k_{\mathrm{r}}', k_{\mathrm{r}}'' = \frac{(k_{\mathrm{r}}+k_{\mathrm{a}}[Gt]+k_{\mathrm{d}}+k_{\mathrm{cat}})}{2} \mp \frac{\sqrt{(k_{\mathrm{r}}+k_{\mathrm{a}}[\mathrm{Gt}]+k_{\mathrm{d}}+k_{\mathrm{cat}})^2-4(k_{\mathrm{d}}+k_{\mathrm{cat}})k_{\mathrm{r}}}}{2} \quad \text{(Eq.12)}$$

The rate of Gt activation is obtained from Eq. 5, Eq. 10 and Eq. 12.

$$\frac{d[\mathrm{Gt}^*]}{dt} = \frac{k_{\mathrm{cat}}[\mathrm{Meta\text{-}II}]_{t=0}^{\mathrm{total}} \times k_{\mathrm{a}}[\mathrm{Gt}]}{\sqrt{(k_{\mathrm{r}}+k_{\mathrm{a}}[\mathrm{Gt}]+k_{\mathrm{d}}+k_{\mathrm{cat}})^2-4(k_{\mathrm{d}}+k_{\mathrm{cat}})k_{\mathrm{r}}}} \times \left(\exp\left(-k_{\mathrm{r}}'t\right) - \exp\left(-k_{\mathrm{r}}''t\right)\right) \quad \text{(Eq. 13)}$$

Therefore, the concentration of Gt* is expressed as follows:

$$[\mathrm{Gt}^*] = \frac{k_{\mathrm{cat}}[\text{Meta-II}]_{t=0}^{\mathrm{total}} \times k_{\mathrm{a}}[\mathrm{Gt}]}{\sqrt{(k_{\mathrm{r}}+k_{\mathrm{a}}[\mathrm{Gt}]+k_{\mathrm{d}}+k_{\mathrm{cat}})^2-4(k_{\mathrm{d}}+k_{\mathrm{cat}})k_{\mathrm{r}}}} \times$$

$$\left(\frac{1}{k_{\mathrm{r}}'}(1-\exp(-k_{\mathrm{r}}'t) - \frac{1}{k_{\mathrm{r}}''}(1-\exp(-k_{\mathrm{r}}''t))\right)$$

(Eq. 14)

The concentration of opsin is expressed as follows using Eq. 11 and Eq. 12

$$[\mathrm{Opsin}] = [\text{Meta-II}]_{t=0}^{\mathrm{total}} \times$$

$$\frac{\{(k_r''-k_r)(1-\exp(-k_{\mathrm{r}}'t))-(k_{\mathrm{r}}'-k_{\mathrm{r}})(1-\exp(-k_{\mathrm{r}}''t))\}}{\sqrt{(k_{\mathrm{r}}+k_{\mathrm{a}}[\mathrm{Gt}]+k_{\mathrm{d}}+k_{\mathrm{cat}})^2-4(k_{\mathrm{d}}+k_{\mathrm{cat}})k_{\mathrm{r}}}}$$

(Eq. 15)

Here we considered two cases in which Meta-II decay is much slower than the association and dissociation of Meta-II·Gt ($k_{\mathrm{r}} << k_{\mathrm{a}}[\mathrm{Gt}], k_{\mathrm{d}}, k_{\mathrm{cat}}$) (i.e. cG) and in which Meta-II decay is comparable to the association and dissociation of Meta-II·Gt (k_{cat}, k_{d}<<k_{a}[Gt], k_{r}), (i.e. mG). If $k_{\mathrm{r}} << k_{\mathrm{a}}[\mathrm{Gt}], k_{\mathrm{d}}$and k_{cat}, Eq. 12 shows that $k_{\mathrm{r}}' << k_{\mathrm{r}}''$ and $k_{\mathrm{r}}'' \approx k_{\mathrm{a}}[\mathrm{Gt}] + k_{\mathrm{d}} + k_{\mathrm{cat}}$. Therefore, the fast component $(\frac{1}{k_{\mathrm{r}}''}(1-\exp(-k_{\mathrm{r}}''t)))$ in Eqs. 14 and 15 is not observable because the present time resolution (100 ms) is lower than k_r''. Thus, Eq. 13 and Eq. 15 become:

$$\frac{d[\mathrm{Gt}^*]}{dt} \approx \frac{k_{\mathrm{cat}}[\text{Meta-II}]_{t=0}^{\mathrm{total}} \times [\mathrm{Gt}]}{[\mathrm{Gt}]+K}\exp(-k_{\mathrm{r}}'t),$$

$$K = \frac{k_{\mathrm{d}}+k_{\mathrm{cat}}}{k_{\mathrm{a}}} \qquad \text{(Eq. 16)}$$

$$[\mathrm{Opsin}] \approx [\text{Meta-II}]_{t=0}^{\mathrm{total}} \times \left(1-\exp\left(-k_{\mathrm{r}}'t\right)\right)$$

(Eq. 17)

On the other hand, if Meta-II decay is rapid (k_{cat}, k_{d}<<k_{a}[Gt], k_{r}), Eq. 12 shows that $k_{\mathrm{r}}' << k_{\mathrm{r}}''$ and $k_{\mathrm{r}}'' \approx k_{\mathrm{a}}[\mathrm{Gt}] + k_{\mathrm{r}}$. Because Meta-II decay of mG was much faster than the present time resolution (see the legend of Fig. 7), the fast component is not observable.

$$\frac{d[\mathrm{Gt}^*]}{dt} \approx \frac{k_{\mathrm{cat}}[\text{Meta-II}]_{t=0}^{\mathrm{total}} \times [\mathrm{Gt}]}{[\mathrm{Gt}]+K}\exp(-k_{\mathrm{r}}'t),$$

$$K = \frac{k_{\mathrm{r}}}{k_{\mathrm{a}}} \qquad \text{(Eq. 18)}$$

$$[\mathrm{Opsin}] \approx [\text{Meta-II}]_{t=0}^{\mathrm{total}} \times$$

$$\frac{k_{\mathrm{r}}+k_{\mathrm{a}}[\mathrm{Gt}](1-\exp(-k_{\mathrm{r}}'t))}{k_{\mathrm{r}}+k_{\mathrm{a}}[\mathrm{Gt}]} \qquad \text{(Eq. 19)}$$

Eq. 16 and Eq. 18 become

$$[\mathrm{Gt}^*] = \frac{k_{\mathrm{cat}}[\text{Meta-II}]_{t=0}^{\mathrm{total}}}{k_{\mathrm{r}}'([\mathrm{Gt}]+K)}(1-\exp(-k_{\mathrm{r}}'t))$$

(Eq. 20)

Eqs. 16, 18 and 20 imply that the concentration change of Gt*, which is progressively decelerated, is expressed by an exponential function with the apparent rate constant of Meta-II decay (k_{r}'). Therefore, while fluorescence increases due to both the opsin formation as well as Gt activation occur for cG and mG, experimentally obtained fluorescence increase is expressed by single exponential function. Florescence increases at time=t for opsin formation ($\Delta F_t^{\mathrm{MII}\rightarrow\mathrm{Ops}}$) and Gt activation ($\Delta F_t^{\mathrm{Gt}\rightarrow\mathrm{Gt}^*}$) are expressed as follows:

$$\Delta F_t^{\mathrm{Gt}\rightarrow\mathrm{Gt}^*} = \Delta F_\infty^{\mathrm{Gt}\rightarrow\mathrm{Gt}^*}(1-\exp(-k_{\mathrm{r}}'t))$$

(Eq. 21)

and

$$\Delta F_t^{\mathrm{MII}\rightarrow\mathrm{Ops}} = \Delta F_\infty^{\mathrm{MII}\rightarrow\mathrm{Ops}}(1-\exp(-k_{\mathrm{r}}'t)),$$

(k_{r}<<k_{a}[Gt], k_{d}, k_{cat}) (Eq. 22)

or

$$\Delta F_t^{\mathrm{MII}\rightarrow\mathrm{Ops}} =$$

$$\Delta F_\infty^{\mathrm{MII}\rightarrow\mathrm{Ops}}\left(\frac{k_{\mathrm{r}}+k_{\mathrm{a}}[\mathrm{Gt}](1-exp(-k_{\mathrm{r}}'t))}{k_{\mathrm{r}}+k_{\mathrm{a}}[Gt]}\right),$$

(k_{cat}, k_{d}<<k_{a}[Gt], k_{r}) (Eq. 23)

The derivatives of Eqs. 21-23 are the rates of fluorescence increases for opsin formation ($V_t^{F(\mathrm{MII}\rightarrow\mathrm{Ops})}$) and Gt activation ($V_t^{F(Gt\rightarrow Gt^*)}$).

$$V_t^{F(\mathrm{Gt}\rightarrow\mathrm{Gt}^*)} = k_\mathrm{r}'\Delta F_\infty^{\mathrm{Gt}\rightarrow\mathrm{Gt}^*}\exp\left(-k_\mathrm{r}'t\right) \quad \text{(Eq. 24)}$$

and

$$V_t^{F(\mathrm{MII}\rightarrow\mathrm{Ops})} = k_\mathrm{r}'\Delta F_\infty^{\mathrm{MII}\rightarrow\mathrm{Ops}}\exp\left(-k_\mathrm{r}'t\right),$$
$$(k_\mathrm{r}<<k_\mathrm{a}[\mathrm{Gt}], k_\mathrm{d}, k_\mathrm{cat}) \quad \text{(Eq. 25)}$$

or

$$V_t^{F(\mathrm{MII}\rightarrow\mathrm{Ops})} = k_\mathrm{r}'\Delta F_\infty^{\mathrm{MII}\rightarrow\mathrm{Ops}}\frac{k_\mathrm{a}[Gt]}{k_\mathrm{r}+k_\mathrm{a}[Gt]}\exp(-k_r't)$$
$$(k_\mathrm{cat}, k_\mathrm{d}<<k_\mathrm{a}[\mathrm{Gt}], k_\mathrm{r}) \quad \text{(Eq. 26)}$$

Therefore, the initial velocity of Gt activation is calculated as follows:

$$V_0^{F(\mathrm{Gt}\rightarrow\mathrm{Gt}^*)} = k_r'(\Delta F_\infty^{\mathrm{total}} - \Delta F_\infty^{\mathrm{MII}\rightarrow\mathrm{Ops}}), \quad \text{(Eq. 27)}$$

where

$$\Delta F_\infty^{\mathrm{total}} = \Delta F_\infty^{\mathrm{Gt}\rightarrow\mathrm{Gt}^*} + \Delta F_\infty^{\mathrm{MII}\rightarrow\mathrm{Ops}} \quad \text{(Eq. 28)}$$

From Eq. 16 and Eq. 18, the initial velocities of Gt activation is plotted against Gt concentration to estimate V_{max} as follows:

$$V_0^{F(\mathrm{Gt}\rightarrow\mathrm{Gt}^*)} = \frac{k_\mathrm{cat}[\mathrm{MetaII}]_{t=0}^{\mathrm{total}}\times[\mathrm{Gt}]}{[\mathrm{Gt}]+K} = V_\mathrm{max}\frac{[\mathrm{Gt}]}{[\mathrm{Gt}]+\mathrm{K}} \quad \text{(Eq. 29)}$$

The concentrations of pigments were 2 or 20 nM in nanodisc samples and 2 nM in ROS samples. The concentrations of GTPγS and Gt were 100 μM and 200-1200 nM, respectively. Gt activation assays were performed in Buffer C.

RESULTS

Pigments in Nanodiscs—In this study, we successfully inserted rhodopsin and cone visual pigments into nanodiscs using CHAPS buffer containing lipids. POPC consists of a palmitoyl group and an oleyl group, which are major components of bovine ROS phosphatidylcholine (33-34). Superdex 200 column chromatography (Fig. 1 insets) demonstrated that the Stoke's diameters of nanodiscs containing bvRh, mRh, cG and mG were 10.7, 10.3, 11.3 and 11.2 nm, respectively, which were in good agreement with previous reports using MSP1E3D1 (14,20). After column chromatography, bvRh, mRh, cG and mG in nanodiscs were further purified by Rho1D4 affinity column chromatography. The absorption spectra of these pigments in nanodiscs are shown in Fig. 1. By using the extinction coefficients of bvRh and MSP, the ratio of MSP to bvRh in nanodiscs was estimated to be 2.2-2.3. This shows that nanodiscs contained monomeric rhodopsin under the experimental conditions. The absorption spectra of cG and mG in nanodiscs showed lower absorbances in the visible region (Figs. 1C-D), indicating that the extinction coefficients of cG and mG in the ultraviolet region (~280 nm) are relatively larger than those of bvRh and mRh. This is consistent with the fact that cG and mG contain more tryptophan and tyrosine residues than bvRh and mRh (Figs. 1A-B).

Comparison of Gt Activation Efficiencies of Rhodopsin and Cone Visual Pigments—Using these rhodopsin and cone visual pigments in nanodiscs, we succeeded in measuring fluorescence changes indicative of Gt activation with high time resolution. Before comparing the Gt activation efficiencies of bvRh, mRh, cG and mG in nanodiscs, we first measured the Gt activation efficiencies of bvRh in ROS and in nanodiscs containing POPC/POPG (POPC/POPG nanodiscs) to examine whether nanodiscs are useful for examining Gt activation efficiencies of visual pigments under physiological conditions (Figs. 2A-B). Initial velocities of Gt activation were calculated and plotted as a function of Gt concentration, and were fitted with the Michaelis-Menten equation to estimate turnover rates of Gt activation by photoactivated pigments, V_{max}/R* (Fig. 2C and Table 1). Initial velocities and V_{max}/R* of bvRh in ROS and nanodiscs were similar, indicating that nanodiscs were useful for estimating Gt activation efficiencies of visual pigments in a membrane environment. Then, we compared the Gt activation efficiencies of bvRh, cG, mRh,

and mG in POPC/POPG nanodiscs at 0-37 °C. Typical fluorescence changes are shown in Figs. 3A-D. The calculated initial velocities of Gt activation were fitted with the Michaelis-Menten equation or Eq. 29 to estimate V_{max}/R^* (Figs. 4A-D and Table 1). V_{max}/R^* of bvRh and mRh were greater than those of cG and mG, indicating that rhodopsin activates Gt more efficiently than cone visual pigments at 0-37 °C. This suggests that rhodopsin activates Gt more efficiently than cone visual pigments under physiological conditions. At 37 °C, V_{max}/R^* of mRh (38.8 Gt*/sec) was about 2.5-fold greater than that of mG (15.4 Gt*/sec). This difference in Gt activation efficiency is consistent with our previous electrophysiological study (*7*), which showed that the amplification efficiency of mRh was about 3-fold greater than that of mG. Therefore, it is likely that the difference in Gt activation efficiency between rhodopsin and cone visual pigments was the main contributor to the difference in the amplification efficiency of the single photon response in that previous study. Additionally, V_{max}/R^* of cG (21.1 Gt*/sec) was about 1.4-fold greater than that of mG (15.4 Gt*/sec) at 37°C. This suggests that different subtypes of cone visual pigments have different Gt activation efficiencies. Moreover, we measured Gt activation efficiencies of bvRh and mG in nanodiscs containing POPC and those containing DOPC/POPG (POPC nanodiscs and DOPC/POPG nanodiscs, respectively) in order to estimate the effect of lipid composition of nanodiscs on the Gt activation efficiency at 37 °C (Fig.5 and Table 2). Vmax/R* of bvRh in POPC and DOPC/POPG nanodiscs were 34.5 and 35.5 Gt*/sec, respectively. Vmax/R* of mG in POPC and DOPC/POPG nanodiscs were 13.6 and 15.9 Gt*/sec, respectively. Vmax/R* in POPC and DOPC/POPG nanodiscs were consistent with those in POPC/POPG nanodiscs.

Estimation of Meta-II Ratio in Equilibrium State of bvRh—In order to estimate the Gt activation efficiencies of Meta-II and characterize the Gt-activating states of rhodopsin and cone visual pigments, we first analyzed the photobleaching processes and estimated the Meta-II ratio in the equilibrium states of bvRh, in which the active state was in equilibrium with the inactive state. Spectral changes of bvRh in ROS, POPC/POPG nanodiscs and DM suspension after light irradiation were measured. We analyzed the difference spectra by singular value decomposition (SVD) and global fitting and obtained b-spectra (Figs. 6A-C) and time constants (data not shown) for the respective kinetic components. We observed bvRh Meta-II formation (b1 and b2) at 0, 10 and 20 °C, and bvRh Meta-II formation (b1) at 37°C in nanodiscs. Additionally, we also observed Meta-II formation (b1 and b2) of bvRh in ROS and DM suspension at 20°C. At 20 °C, the time constants of Meta-II formation for recombinant bvRh in POPC/POPG nanodiscs (6.23 ms and 47.7 ms) were similar to those of native bvRh in ROS (8.65 ms and 37.8 ms), like those of native bvRh in nanodiscs (*35*). At this time scale, decay of Meta-II was not observed. Therefore, the b0 spectrum, which is the spectrum extrapolated to infinite time, shows the equilibrium between Meta-I and Meta-II (Fig.6D). Using this b0 spectrum, the fraction of Meta-II in Meta-I/Meta-II equilibrium ($F_{\text{Meta-II}}$) was estimated as previously described (36-37) (Table 3). $F_{\text{Meta-II}}$ in nanodiscs was 51 % at 20 °C, which was consistent with that in ROS (57 %), whereas $F_{\text{Meta-II}}$ in DM-solubilized bvRh is 100%, which is considerably higher than $F_{\text{Meta-II}}$ in nanodiscs and ROS. The same analysis at various temperatures showed that $F_{\text{Meta-II}}$ was sensitive to temperature (Table 3).

Estimation of Meta-II Ratios in Equilibrium State of cG and mG—We also analyzed the photobleaching processes to estimate the Meta-II ratios of cG and mG in POPC/POPG nanodiscs, although this analysis was more complicated. Spectral changes after photon absorption were measured and analyzed by SVD and global fitting at 0-37 °C. From the SVD analysis, b-spectra (Fig. 7A-B) and time constants (data not shown) were obtained. At 0 and 10 °C, we observed Meta-I→Meta-II+Meta-III (b1 and b2 at 0 and 10 °C, b1 at 20 and 37 °C) and Meta-II→opsin (b3 at 0 and 10°C, b2 at 20 and 37 °C) and Meta-III→opsin (b4 at 0 and 10 °C, b3 at 20 and 37 °C) of cG. This is consistent with the photobleaching process of cG in DM suspension (*30*). On the other hand, we observed Meta-I→Meta-II+Meta-III (b1), and Meta-II→opsin (b2) and Meta-III→opsin (b3) of mG at 10-37 °C, which is consistent with photobleaching process of cG. Then, in order to

estimate the ratios of Meta-I, Meta-II, and Meta-III in the equilibria of these intermediates for cG and mG, we calculated model spectra of these intermediates by using the b-spectra obtained. The model absorption spectrum of the dark state ([Dark]) of cG or mG was constructed using the difference spectra before and after light exposure in the presence of hydroxylamine, as previously reported (*38*).

The model spectra of intermediates of cG and mG were calculated using the model spectra of the dark state and the b-spectra of cG at 0°C, or those of mG at 10 °C. Meta-I spectrum ([Meta-I]) was calculated as follows:

$$[\text{Meta-I}] = [\text{Dark}] + B_{t=0}/f_d$$

(f_d ; the fraction of the photoactivated pigment)

where $B_{t=0}$ is the difference spectrum at t=0

$$B_{t=0} = b0 - b1 - b2 - b3 - b4 \ \text{(cG)}$$

$$B_{t=0} = b0 - b1 - b2 - b3 \ \text{(mG)}$$

[Meta-III] was calculated as follows:

$$[\text{Meta-III}] = [\text{Dark}] + b0/f_d - b4/f_3 \ \text{(cG)}$$

$$[\text{Meta-III}] = [\text{Dark}] + b0/f_d - b3/f_3 \ \text{(mG)}$$

where f_3 is the fraction of Meta-III, which was determined such that b0 cancels the absorbance at 380 nm in b4 (cG) or b3 (mG). [Meta-II] was calculated as follows:

$$[\text{Meta-II}] = ([\text{Meta-I}] - \frac{b1}{f_2} + \frac{[\text{Meta-I}] - [\text{Meta-III}]}{f_3})/(1 - f_3)$$

where f_2 is the fraction of Meta-II, which was determined such that b1 cancels the absorbance at 480 nm.

The calculated α-bands of intermediates were fitted by retinoid curves, and β-bands were fitted by Gaussian curves as previously described (*38*). Figs. 7C and D show the calculated model spectra of the dark state and intermediates of cG and mG, respectively.

The fraction of Meta-III ($F_{\text{Meta-III}}$) was estimated by using b4 spectra for cG at 0 and 10 °C, or b3 spectra for cG at 20 and 37 °C and for mG, which reflect the decay of Meta-III, and model spectra of Meta-III (Table 4). We then calculated difference spectra (B_{eq}) obtained when the equilibrium between Meta-I, Meta-II and Meta-III is formed as follows (Figs. 7E-F):

$$B_{eq} = b0 - b3 - b4 \ \text{(cG at 0 and 10 °C)}$$

$$B_{eq} = b0 - b2 - b3$$

(cG at 20 and 37 °C, and mG)

They were fitted with the model spectra to estimate the fractions of Meta-I, Meta-II and Meta-III in the equilibrium (Table 4). The $F_{\text{Meta-II}}$ of cG and mG were increased at higher temperature, like that of bvRh, although $F_{\text{Meta-II}}$ of mG was smaller than that of cG. At 37 °C, $F_{\text{Meta-II}}$ of bvRh (74%) was similar to that of cG (74%) and greater than that of mG (41%).

Gt Activation Efficiencies of Meta-II—To compare the nature of the Gt-activating state (Meta-II) generated by photoactivation of rod and cone visual pigments, we estimated the turnover rates of the activation of Gt by Meta-II (V_{max}/MII) of bvRh, cG and mG using $F_{\text{Meta-II}}$ (Tables 3-4), and listed them in Table 1. V_{max}/MII of bvRh in POPC/POPG nanodiscs (22.0 Gt*/sec) was consistent with that of bvRh in ROS (24.2 Gt*/sec), like V_{max}/R*. V_{max}/MII of bvRh (52.2 Gt*/sec at 37 °C) was greater than V_{max}/MII of cG (28.5Gt*/sec at 37°C) and mG (37.6 Gt*/sec at 37 °C) in POPC/POPG nanodiscs, indicating that rhodopsin forms more efficient Gt-activating states, which finally cause the higher V_{max}/R* of rhodopsin. Vmax/MII of bvRh and cG measured at 4 temperatures (0, 10, 20, 37 °C) were then plotted in the Arrhenius manner (Fig. 8) and the apparent activation energy (Ea) was calculated to be 38 kJ/mol for cG and 22 kJ/mol for bvRh. Vmax/MII of mG measured at 20 and 37 °C were also plotted in Fig. 8, showing that the Ea of mG would be similar to that of cG. These results suggested that Ea of cone visual pigments is about 2-fold greater than that of rhodopsin.

DISCUSSION

In this study, we compared Gt activation efficiencies of rod and cone visual pigments in a membrane environment at physiological temperature with high time resolution using a fluorescence assay (Figs. 2-3). Rhodopsin showed about 2-3-fold higher Gt activation efficiencies than cone visual pigments (Figs. 4-5

and Tables 1-2). Moreover, the specific Gt activation efficiency of Meta-II formed from rhodopsin was higher than that of Meta-II formed from cone visual pigments (Fig. 8).

Nanodiscs Mimic Native Membrane Environments—We confirmed that bvRh in POPC/POPG nanodiscs showed similar properties to bvRh in native ROS membranes (Fig. 2 and Table 1). Our data indicated that V_{max}/R^*, V_{max}/MII and $F_{Meta\text{-}II}$ of photoactivated bvRh in nanodiscs were in good agreement with those of bvRh in ROS (Tables 1 and 3), which is consistent with previous studies (18,35). Thus, these results demonstrated that nanodiscs mimic the native membrane environment and that the above-mentioned molecular properties of visual pigments in the physiological environment can be studied using nanodisc samples.

Gt Activation Efficiencies of Rhodopsin and Cone Visual Pigments—In this study, we measured the initial velocities of Gt activation at different Gt concentrations at 0-37 °C to estimate the activation efficiencies (turnover rates of photoactivated pigments; V_{max}/R^*) of bvRh, mRh, cG, and mG (Figs. 4-5 and Tables 1-2) in nanodiscs. Our fluorescence assay showed that V_{max}/R^* of bvRh and mRh were greater than those of cG and mG at 0-37 °C. It should be noted that this finding is inconsistent with previous reports showing that the initial velocity of Gt activation by cone visual pigments was similar to that of rhodopsin (7,9-10). The previous studies were performed in the presence of about a 10-fold excess of Gt using the pigments in liposomes or native membranes at 0 or 4 °C. We assessed the dependence of V_{max}/R^* on Gt concentration and showed that the initial velocities of cG and bvRh were very similar in the presence of a 10-fold excess of Gt relative to visual pigment (Fig. 4). Our data are also consistent with a recent report that rhodopsin exhibits about 2-times more efficient G protein activation as compared to cone visual pigments at 20 °C in a poikilothermic animal (carp) (*11*). While we used rod Gt α-subunit in the present assay, it has been suggested that rod and cone Gt α-subunits are functionally interconvertible *in vivo* and *in vitro* (*39-41*).

Contribution of Gt Activation Efficiencies of Visual Pigments to Photoresponses of Rods and Cones—Electrophysiological analyses indicated that the amplification efficiency for the single photon response of rods of wild-type mice was about 3-fold greater than that of mG knock-in mice (*7*). This difference is explained by the difference in V_{max}/R^* of Gt activation between mRh and mG at 37 °C. In the previous studies, the amplification efficiency of the transduction cascade per bleached pigment in mouse rods was about 6.8-fold higher than that in mouse cones (7-8). Taken together, that finding combined with the present results suggest that about half of the difference in signal amplification between rods and cones is caused by the difference between the Gt activation efficiencies of rhodopsin and cone visual pigments. We confirmed that the native rod membrane environment can be mimicked by the method using POPC/POPG nanodiscs. However, we cannot completely exclude the possibility that Gt activation efficiency of the reconstituted cone visual pigments in nanodiscs is different from that of the cone visual pigments in native cone membranes because the lipid composition of nanodiscs (POPC/POPG) was different from that in the native cone membranes. It is extremely hard at present time to isolate cone outer segments containing mG from rod outer segments in mouse retinas, because about 98% of photoreceptor cells in the retinas are rod photoreceptor cells. Also, it is impracticable to isolate lipids from cone outer segments to prepare nanodisc containing native lipids. Therefore, we have tried to estimate the effect of lipid composition on the Gt activation efficiency. Yuan et al. reported that the lipid composition of gecko photoreceptor outer segment membranes that contain cone-type pigments contained more negatively charged and unsaturated phospholipids than rods (*42*). Therefore we prepared nanodisc sample containing only POPC and that containing the mixture of DOPC and POPG at the ratio of 3:2 (DOPC/POPG), to change the contents of negative charges and unsaturation of the lipids and measure Gt activation efficiencies of bvRh and mG (Fig. 5 and Table 2). The results indicated that the Gt activation efficiencies of bvRh and mG are independent of lipid composition, confirming that the difference in Gt activation efficiency between rhodopsin and cone visual pigments is lipid-independent. However, it was also reported that the amplitude of the single photon response of *Xenopus* rods in which human or salamander red-sensitive cone

visual pigment was expressed was similar (less than 2-fold difference) to that of *Xenopus* rods in which *Xenopus* or human rhodopsin was expressed (*43*). The discrepancy between that report and our present findings could be due to the difference in the temperature of measurements or to the presence of A2-retinal in the *Xenopus* retina. Therefore, in the future, it will be important to measure the Gt activation efficiencies of *Xenopus* and human rhodopsin, human red and salamander red reconstituted with A2-retinal at about 20 °C by using nanodisc samples.

Gt-activating States of Rhodopsin and Cone Visual Pigments—In order to characterize the Gt-activating state (Meta-II) of rhodopsin and cone visual pigments, we analyzed their photobleaching processes and estimated $F_{Meta\text{-}II}$ in their equilibrium states in POPC/POPG nanodiscs (Tables 3-4). The specific Gt activation efficiency of Meta-II (V_{max}/MII) was calculated using V_{max}/R* and $F_{Meta\text{-}II}$. V_{max}/MII of rhodopsin was greater than those of cone visual pigments (Table 1 and Fig. 8), which was also consistent with the different amplification efficiency between rods and cones.

In all the experiments presented here, bovine rod Gt was used. Although V_{max}/MII of bvRh was greater than that of cG, the amino acid residues of the second and third cytoplasmic loops of both pigments, which interact with Gt (44), are well conserved. Thus, it is suggested that the different Gt activation efficiencies of rhodopsin and cone visual pigments derive from differences of the conformation of their Meta-II complex with Gt. Arrhenius plots (Fig. 8) indicated that the activation energy (Ea) of cone visual pigments was about 2-fold greater than that of rhodopsin. This implies that the activation of Gt by Meta-II of cone visual pigments requires greater enthalpy than that by Meta-II of rhodopsin. These findings suggest that there is some difference in the hydrogen bond(s) and/or hydrophobic bond(s) involved in the interaction between Gt and Meta-II.

Properties of Different Subtypes of Cones—Our analysis found not only a difference in Gt activation efficiencies between rhodopsin and cone visual pigments, but also a difference between different subtypes of cone visual pigments (cG and mG). $F_{Meta\text{-}II}$ of mG (L group) was smaller than that of cG (M2 group), and thus V_{max}/R* of mG was lower than that of cG at 37 °C, although their V_{max}/MII values were comparable. The photoresponses of M-cones and S-cones in mouse are very similar but not identical (*8*). Because the subtypes of Gt, PDE and other functional proteins are the same in cones, it is likely that the different photoresponses among cones mainly depend on the different molecular properties of cone visual pigments. The molecular basis of the photoresponses of cones will be clarified by further analyses of the molecular properties of functional proteins, including visual pigments in nanodiscs.

In summary, we showed differences in the Gt activation efficiencies of rhodopsin and cone visual pigments using nanodiscs that mimic the native membrane environment. The difference in Gt activation efficiencies between rhodopsin and cone visual pigments is quantitatively consistent with the different amplification efficiency between rods and cones. The specific Gt activating efficiency of the active state of rhodopsin is greater than that of cone visual pigments. Rhodopsin appears to have acquired these molecular properties of its active state during the process of its evolution from a cone visual pigment so as to increase its G protein activation efficiency.

REFERENCES

1. Fu, Y., and Yau, K. W. (2007) Phototransduction in mouse rods and cones. *Pflugers Arch* **454**, 805-819
2. Kawamura, S., and Tachibanaki, S. (2008) Rod and cone photoreceptors: molecular basis of the difference in their physiology. *Comp Biochem Physiol A Mol Integr Physiol* **150**, 369-377
3. Yau, K. W. (1994) Phototransduction mechanism in retinal rods and cones. The Friedenwald Lecture. *Invest Ophthalmol Vis Sci* **35**, 9-32
4. Ebrey, T., and Koutalos, Y. (2001) Vertebrate photoreceptors. *Prog Retin Eye Res* **20**, 49-94
5. Arshavsky, V. Y., Lamb, T. D., and Pugh, E. N., Jr. (2002) G proteins and phototransduction. *Annu Rev Physiol* **64**, 153-187
6. Shichida, Y., and Imai, H. (1998) Visual pigment: G-protein-coupled receptor for light signals. *Cell Mol Life Sci* **54**, 1299-1315
7. Sakurai, K., Onishi, A., Imai, H., Chisaka, O., Ueda, Y., Usukura, J., Nakatani, K., and Shichida, Y. (2007) Physiological properties of rod photoreceptor cells in green-sensitive cone pigment knock-in mice. *J Gen Physiol* **130**, 21-40
8. Nikonov, S. S., Kholodenko, R., Lem, J., and Pugh, E. N., Jr. (2006) Physiological features of the S- and M-cone photoreceptors of wild-type mice from single-cell recordings. *J Gen Physiol* **127**, 359-374
9. Fukada, Y., Okano, T., Artamonov, I. D., and Yoshizawa, T. (1989) Chicken red-sensitive cone visual pigment retains a binding domain for transducin. *FEBS Lett* **246**, 69-72
10. Imai, H., Terakita, A., Tachibanaki, S., Imamoto, Y., Yoshizawa, T., and Shichida, Y. (1997) Photochemical and biochemical properties of chicken blue-sensitive cone visual pigment. *Biochemistry* **36**, 12773-12779
11. Tachibanaki, S., Yonetsu, S., Fukaya, S., Koshitani, Y., and Kawamura, S. (2012) Low activation and fast inactivation of transducin in carp cones. *J Biol Chem* **287**, 41186-41194
12. Tachibanaki, S., Tsushima, S., and Kawamura, S. (2001) Low amplification and fast visual pigment phosphorylation as mechanisms characterizing cone photoresponses. *Proc Natl Acad Sci U S A* **98**, 14044-14049
13. Shi, G., Yau, K. W., Chen, J., and Kefalov, V. J. (2007) Signaling properties of a short-wave cone visual pigment and its role in phototransduction. *J Neurosci* **27**, 10084-10093
14. Denisov, I. G., Grinkova, Y. V., Lazarides, A. A., and Sligar, S. G. (2004) Directed self-assembly of monodisperse phospholipid bilayer Nanodiscs with controlled size. *J Am Chem Soc* **126**, 3477-3487
15. Ritchie, T. K., Grinkova, Y. V., Bayburt, T. H., Denisov, I. G., Zolnerciks, J. K., Atkins, W. M., and Sligar, S. G. (2009) Chapter 11 - Reconstitution of membrane proteins in phospholipid bilayer nanodiscs. *Methods Enzymol* **464**, 211-231
16. Kuszak, A. J., Pitchiaya, S., Anand, J. P., Mosberg, H. I., Walter, N. G., and Sunahara, R. K. (2009) Purification and functional reconstitution of monomeric mu-opioid receptors: allosteric modulation of agonist binding by Gi2. *J Biol Chem* **284**, 26732-26741
17. Bayburt, T. H., and Sligar, S. G. (2010) Membrane protein assembly into Nanodiscs. *FEBS Lett* **584**, 1721-1727
18. Whorton, M. R., Jastrzebska, B., Park, P. S., Fotiadis, D., Engel, A., Palczewski, K., and Sunahara, R. K. (2008) Efficient coupling of transducin to monomeric rhodopsin in a phospholipid bilayer. *J Biol Chem* **283**, 4387-4394
19. Bayburt, T. H., Leitz, A. J., Xie, G., Oprian, D. D., and Sligar, S. G. (2007) Transducin activation by nanoscale lipid bilayers containing one and two rhodopsins. *J Biol Chem* **282**, 14875-14881
20. Tsukamoto, H., Sinha, A., DeWitt, M., and Farrens, D. L. (2010) Monomeric rhodopsin is the minimal functional unit required for arrestin binding. *J Mol Biol* **399**, 501-511
21. Bayburt, T. H., Vishnivetskiy, S. A., McLean, M. A., Morizumi, T., Huang, C. C., Tesmer, J. J., Ernst, O. P., Sligar, S. G., and Gurevich, V. V. (2011) Monomeric rhodopsin is sufficient for

normal rhodopsin kinase (GRK1) phosphorylation and arrestin-1 binding. *J Biol Chem* **286**, 1420-1428

22. Whorton, M. R., Bokoch, M. P., Rasmussen, S. G., Huang, B., Zare, R. N., Kobilka, B., and Sunahara, R. K. (2007) A monomeric G protein-coupled receptor isolated in a high-density lipoprotein particle efficiently activates its G protein. *Proc Natl Acad Sci U S A* **104**, 7682-7687
23. Okano, T., Kojima, D., Fukada, Y., Shichida, Y., and Yoshizawa, T. (1992) Primary structures of chicken cone visual pigments: vertebrate rhodopsins have evolved out of cone visual pigments. *Proc Natl Acad Sci U S A* **89**, 5932-5936
24. Yokoyama, S. (2008) Evolution of dim-light and color vision pigments. *Annu Rev Genomics Hum Genet* **9**, 259-282
25. Shichida, Y., and Matsuyama, T. (2009) Evolution of opsins and phototransduction. *Philos Trans R Soc Lond B Biol Sci* **364**, 2881-2895
26. Morizumi, T., Imai, H., and Shichida, Y. (2003) Two-step mechanism of interaction of rhodopsin intermediates with the C-terminal region of the transducin alpha-subunit. *J Biochem* **134**, 259-267
27. Sato, K., Yamashita, T., Imamoto, Y., and Shichida, Y. (2012) Comparative studies on the late bleaching processes of four kinds of cone visual pigments and rod visual pigment. *Biochemistry* **51**, 4300-4308
28. Kuwayama, S., Imai, H., Morizumi, T., and Shichida, Y. (2005) Amino acid residues responsible for the meta-III decay rates in rod and cone visual pigments. *Biochemistry* **44**, 2208-2215
29. Banerjee, S., Huber, T., and Sakmar, T. P. (2008) Rapid incorporation of functional rhodopsin into nanoscale apolipoprotein bound bilayer (NABB) particles. *J Mol Biol* **377**, 1067-1081
30. Imamoto, Y., Seki, I., Yamashita, T., and Shichida, Y. (2013) Efficiencies of activation of transducin by cone and rod visual pigments. *Biochemistry* **52**, 3010-3018
31. Imamoto, Y., and Shichida, Y. (2008) Thermal recovery of iodopsin from photobleaching intermediates. *Photochem Photobiol* **84**, 941-948
32. Tachibanaki, S., Imai, H., Mizukami, T., Okada, T., Imamoto, Y., Matsuda, T., Fukada, Y., Terakita, A., and Shichida, Y. (1997) Presence of two rhodopsin intermediates responsible for transducin activation. *Biochemistry* **36**, 14173-14180
33. Anderson, R. E., and Maude, M. B. (1970) Phospholipids of bovine outer segments. *Biochemistry* **9**, 3624-3628
34. Albert, A. D., Young, J. E., and Paw, Z. (1998) Phospholipid fatty acyl spatial distribution in bovine rod outer segment disk membranes. *Biochim Biophys Acta* **1368**, 52-60
35. Tsukamoto, H., Szundi, I., Lewis, J. W., Farrens, D. L., and Kliger, D. S. (2011) Rhodopsin in Nanodiscs Has Native embrane-like Photointermediates. *Biochemistry* **50**, 5086-5091
36. Sato, K., Morizumi, T., Yamashita, T., and Shichida, Y. (2010) Direct observation of the pH-dependent equilibrium between metarhodopsins I and II and the pH-independent interaction of metarhodopsin II with transducin C-terminal peptide. *Biochemistry* **49**, 736-741
37. Morizumi, T., Imai, H., and Shichida, Y. (2005) Direct observation of the complex formation of GDP-bound transducin with the rhodopsin intermediate having a visible absorption maximum in rod outer segment membranes. *Biochemistry* **44**, 9936-9943
38. Matsuyama, T., Yamashita, T., Imamoto, Y., and Shichida, Y. (2012) Photochemical properties of mammalian melanopsin. *Biochemistry* **51**, 5454-5462
39. Deng, W. T., Sakurai, K., Liu, J., Dinculescu, A., Li, J., Pang, J., Min, S. H., Chiodo, V. A., Boye, S. L., Chang, B., Kefalov, V. J., and Hauswirth, W. W. (2009) Functional interchangeability of rod and cone transducin alpha-subunits. *Proc Natl Acad Sci U S A* **106**, 17681-17686
40. Gopalakrishna, K. N., Boyd, K. K., and Artemyev, N. O. (2012) Comparative analysis of cone and rod transducins using chimeric Galpha subunits. *Biochemistry* **51**, 1617-1624
41. Mao, W., Miyagishima, K. J., Yao, Y., Soreghan, B., Sampath, A. P., and Chen, J. (2013) Functional comparison of rod and cone Galpha(t) on the regulation of light sensitivity. *J Biol*

Chem **288**, 5257-5267

42. Yuan, C., Chen, H., Anderson, R. E., Kuwata, O., and Ebrey, T. G. (1998) The unique lipid composition of gecko (Gekko Gekko) photoreceptor outer segment membranes. *Comp Biochem Physiol B Biochem Mol Biol* **120**, 785-789
43. Kefalov, V., Fu, Y., Marsh-Armstrong, N., and Yau, K. W. (2003) Role of visual pigment properties in rod and cone phototransduction. *Nature* **425**, 526-531
44. Konig, B., Arendt, A., McDowell, J. H., Kahlert, M., Hargrave, P. A., and Hofmann, K. P. (1989) Three cytoplasmic loops of rhodopsin interact with transducin. *Proc Natl Acad Sci U S A* **86**, 6878-6882
45. Tachibanaki, S., Imai, H., Terakita, A., and Shichida, Y. (1998) Identification of a new intermediate state that binds but not activates transducin in the bleaching process of bovine rhodopsin. *FEBS Lett* **425**, 126-130

Acknowledgments–We thank Dr. S. Koike for providing us with HEK293T cell lines and Prof. R. S. Molday for the generous gift of a Rho1D4-producing hybridoma. We are also grateful to Dr. Elizabeth Nakajima and Take Matsuyama for critical reading of our manuscript and invaluable comments.

FOOTNOTES

*This work was supported by the Japanese Ministry of Education, Culture, Sports, Science, and Technology (Grants-in-aid for Scientific Research to Y. I. (23370070), T. Y. (25440167), and Y. S. (25251036), and Grants for Excellent Graduate Schools).
[1]To whom correspondence should be addressed: Yoshinori Shichida, Department of Biophysics, Graduate School of Science, Kyoto University, Kyoto 606-8502, Japan, Tel.: +81-75-753-4213; Fax: +81-75-753-4210; E-mail: shichida@rh.biophys.kyoto-u.ac.jp.
[2]The abbreviations used are:
GPCR, G protein coupled receptor
GTPγS, guanosine 5-3-*O*-(thio)triphosphate
ROS, rod outer segment
Gt, transducin
CHAPS, 3-[(3-Cholamidopropyl)dimethylammonio]propanesulfonate
HEPES, 4-(2-hydroxyethyl)-1-piperazineethanesulfonic acid
POPC, 1-palmitoyl-2-oleoyl-*sn*-glycero-3-phosphocholine
POPG, 1-palmitoyl-2-oleoyl-*sn*-glycero-3-phospho-(1'-*rac*-glycerol)
DOPC, 1,2-dioleoyl-phosphatidylcholine
Tris, tris(hydroxymethyl)aminomethane
EDTA, 2-({2-[bis(carboxymethyl)amino]ethyl}(carboxymethyl)amino)acetic acid
DM, n-Dodecyl-β-D-maltoside
Meta-I, Meta-II and Meta-III, bleaching intermediates of cone visual pigments corresponding to metarhodopsin I, metarhodopisn II and metarhodopsin III, respectively.

FIGURE LEGENDS

FIGURE 1. Absorption spectra of bvRh (A), mRh (B), cG (C) and mG (D) in POPC/POPG nanodiscs. The spectra were measured at 0 °C. The insets show chromatograms of nanodisc size exclusion. We collected the peak fraction at 10.5-12.5 mL corresponding to the Stoke's diameters of nanodiscs containing pigments.

FIGURE 2. Comparison of Gt activation efficiencies of bvRh in ROS and nanodiscs.
(A) Gt activation by photoactivated bvRh in POPC/POPG nanodiscs. 2 nM pigment was mixed with 400 nM Gt and 100 μM GTPγS at 20°C. The mixture was irradiated with a yellow flash at time=0 and the fluorescence intensity was monitored (upper traces). Fluorescence increase originated from the opsin formation was monitored in the absence of Gt at 20°C (lower traces). (B) Gt activation by photoactivated bvRh in ROS. 2 nM pigment was mixed with 400 nM Gt and 100 μM GTPγS at 20 °C. The mixture was irradiated with a yellow flash at time=0 and the fluorescence intensity was monitored (upper traces). The fluorescence increase that resulted from the opsin formation was monitored in the absence of Gt at 20 °C (lower traces). (C) Initial velocities of Gt activation by photoactivated bvRh in ROS and POPC/POPG nanodiscs at 20 °C (open triangles and filled squares, respectively). Plots of initial velocities were fitted by the Michaelis-Menten equation (solid line for ROS and dashed line for nanodiscs). Error bars represent the standard deviations estimated from three independent measurements.

FIGURE 3. Gt activation by photoactivated bvRh (A), mRh (B), cG (C) and mG (D) in POPC/POPG

nanodiscs. 20 nM pigment was mixed with 400 nM Gt and 100 μM GTPγS at 37 °C. The mixture was irradiated with a yellow flash at time=0 and the fluorescence intensity was monitored (upper traces). Fluorescence increase that originated from the opsin formation was monitored in the absence of Gt at 37 °C (lower traces).

FIGURE 4. Initial velocities of Gt activation by photoactivated pigments in POPG/POPG nanodiscs. Initial velocities of bvRh, cG, mRh and mG (closed squares, closed circles, open squares and open circles, respectively) at 0 °C (A), 10 °C (B), 20 °C (C) and 37 °C (D) were plotted against Gt concentration, and fitted by the Michaelis-Menten equation or Eq. 29 (solid lines for bvRh and mG, dashed lines for mRh and cG) to estimate V_{max}/R^*. Error bars represent the standard deviations estimated from three independent measurements.

FIGURE 5. Initial velocities of Gt activation by photoactivated bvRh (A), and mG (B) in POPC/POPG, POPC and DOPC/POPG nanodiscs. Initial velocities of bvRh and mG in POPC/POPG , POPC and DOPC/POPG nanodiscs (closed squares, closed circles and closed triangles, respectively) at 37 °C were plotted against Gt concentration, and fitted by the Michaelis-Menten equation or Eq. 29 (solid lines for POPC/POPG nanodiscs, dashed lines for POPC nanodiscs and dotted lines for DOPC/POPG nanodiscs) to estimate V_{max}/R^*. Error bars represent the standard deviations estimated from three independent measurements.

FIGURE 6. Photobleaching processes and estimation of Meta-II ratios of bvRh. The b-spectra of bvRh in POPC/POPG nanodiscs at 20 °C (A), in ROS at 20 °C (B), and in DM suspension at 20 °C (C) calculated by SVD analysis are presented. The b-spectra of bvRh in nanodiscs at 0 and 10 °C were consistent with those at 20 °C. B1 spectrum of bvRh in nanodiscs at 37°C was consistent with that at 20 °C. Two-step formation of Meta-II (b1 and b2) is consistent with previous reports that suggested the presence of two forms of Meta-I (Meta-Ia and Meta-Ib) (32,45). B0 spectra, which were difference spectra in the equilibrium state, of bvRh in nanodiscs and ROS and DM suspension are shown in (D). Solid lines for bvRh in nanodiscs at 0-37 °C, and dashed lines for bvRh in ROS or DM suspension at 20 °C. These spectra were fitted by Meta-I and Meta-II model spectra as previously described (36-37) to estimate $F_{Meta\text{-}II}$ (Table 3).

FIGURE 7. Photobleaching processes and estimation of Meta-II ratios of cG and mG in POPC/POPG nanodiscs. (A) B-spectra calculated by SVD analysis of cG in nanodiscs at 20 °C. At 0 and 10 °C, b1 and b2 spectra were consistent with b1 at 20 °C, and b3 and b4 were consistent with b2 and b3 at 20 °C respectively. At 37 °C, b-spectra were consistent with those at 20 °C. (B) B-spectra calculated by SVD analysis of mG in nanodiscs at 20 °C. At 10 and 37 °C, the b-spectra were consistent with those at 20 °C. The time constants of b1, b2 and b3 were 4.9 ms, 79 ms and 4.6 sec, respectively at 20 °C. (C) Model absorption spectra of dark state and photobleaching intermediates of cG. Absorption maxima of cG were 508 nm for dark state, 483 nm for Meta-I, 374 nm for Meta-II, and 465 nm for Meta-III. (D) Model absorption spectra of dark state and photobleaching intermediates of mG. Absorption maxima of mG were 513 nm for dark state, 479 nm for Meta-I, 378 nm for Meta-II, and 479 nm for Meta-III. For details, see text. (E) Calculated difference spectra (B_{eq}) of equilibrium states of cG at 0-37 °C. These spectra were fitted by model dark state, Meta-I, Meta-II and Meta-III spectra to estimate $F_{Meta\text{-}II}$ (Table 4). (F) Calculated difference spectra (B_{eq}) in equilibrium states of mG at 10-37 °C. These spectra were also fitted by the model spectra to estimate $F_{Meta\text{-}II}$ (Table 4).

FIGURE 8. Arrhenius plots of turnover rates (V_{max}/MII) of Gt activation by bvRh, cG and mG (closed squares, closed circles and open circles, respectively) in POPC/POPG nanodiscs. Plots of bvRh and cG were fitted by straight lines (solid and dashed lines, respectively) to calculate apparent activation energy (E_a).

TABLES

Table 1: Kinetic Parameters[a] of Gt Activation by Rhodopsin and Cone Visual Pigments

Sample	Temperature (°C)	V_{max}/R* (sec^{-1})	V_{max}/Meta-II (sec^{-1})	K_M or K (nM)
ROS*	20	13.8 ± 0.9	24.2 ± 1.5	774 ± 60
bvRh/nanodisc*	20	11.9±1.3	23.3 ± 2.5	718 ± 152
bvRh/nanodisc	0	2.42 ± 0.27	17.3 ± 1.9	638 ± 227
	10	5.42 ± 0.98	17.5 ± 3.2	465 ± 117
	20	11.2 ± 1.7	22.0 ± 3.3	595 ± 45
	37	38.6 ± 3.3	52.2 ± 4.5	1158 ± 120
mRh/nanodisc	20	11.3 ± 1.6	nd	731 ± 142
	37	38.8 ± 1.2	nd	856 ± 124
cG/nanodisc	0	1.56 ± 0.21[b]	3.90 ± 0.53[d]	363 ± 108
	10	3.96 ± 0.24[b]	7.62 ± 0.46[d]	841 ± 89
	20	8.21 ± 0.79[b]	13.5 ± 1.3[d]	932 ± 45
	37	21.1 ± 1.9[b]	28.5 ± 2.6[d]	901 ± 130
mG/nanodisc	20	4.73 ± 0.69[b,c]	12.1 ± 1.8[d]	1068 ± 177
	37	15.4 ± 1.2[b,c]	37.6 ± 3.0[d]	794 ± 153

[a]Values are shown as average ± standard deviation calculated from three independent measurements. [b]Significantly different from V_{max}/R* of bvRh and mRh at the same temperature (p<0.05). [c]Significantly different from V_{max}/R* of cG at the same temperature (p<0.05). [d]Significantly different from V_{max}/Meta-II of bvRh at the same temperature (p<0.05). *The concentration of bvRh was 2 nM. In other experiments, the concentrations of pigments were 20 nM. Lipid composition of nanodiscs was the mixture of POPC/POPG at the ratio of 3:2 (POPC/POPG).

Table 2: Kinetic Parameters[a] of Gt Activation by Rhodopsin and Cone Visual Pigments

Sample	Lipid	V_{max}/R* (sec^{-1})	K_M or K (nM)
bvRh/nanodisc	POPC/POPG	35.3 ± 4.7	994 ± 172
	POPC	34.5 ± 3.8	816 ± 229
	DOPC/POPG	35.5 ± 2.8	897 ± 167
mG/nanodisc	POPC/POPG	15.4 ± 1.2	794 ± 153
	POPC	13.6 ± 1.3	848 ± 292
	DOPC/POPG	15.9 ± 1.0	868 ± 179

[a]Values are shown as average ± standard deviation calculated from three independent measurements. The concentrations of pigments were 20 nM. The experiments were performed at 37 °C.

Table 3: Fraction of Meta-II in the Equilibrium of Rhodopsin

Sample	Temperature (°C)	$F_{Meta-II}$ (%)
bvRh/nanodisc	0	14
	10	31
	20	51
	37	74
bvRh/DM	20	100
ROS	20	57

Table 4: Fraction of Meta Intermediates in the Equilibrium of Cone Visual Pigments

Sample	Temperature (°C)	F_{Meta-I} (%)	$F_{Meta-II}$ (%)	$F_{Meta-III}$ (%)
cG/nanodisc	0	52	40	8
	10	38	52	10
	20	31	61	7
	37	15	74	12
mG/nanodisc	10	48	27	25
	20	39	39	22
	37	29	41	30

Scheme 1: Michaelis-Menten Model for Gt Activation by Photoactivated Pigments.

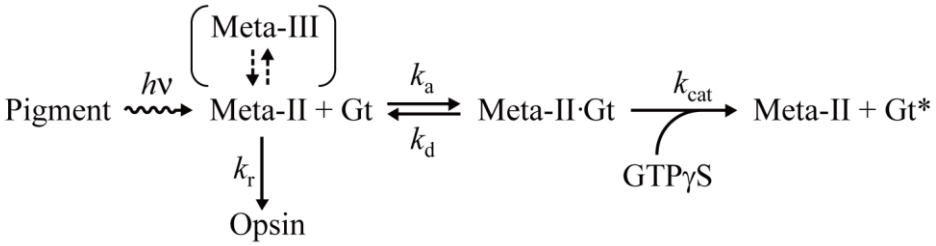

Fig.1

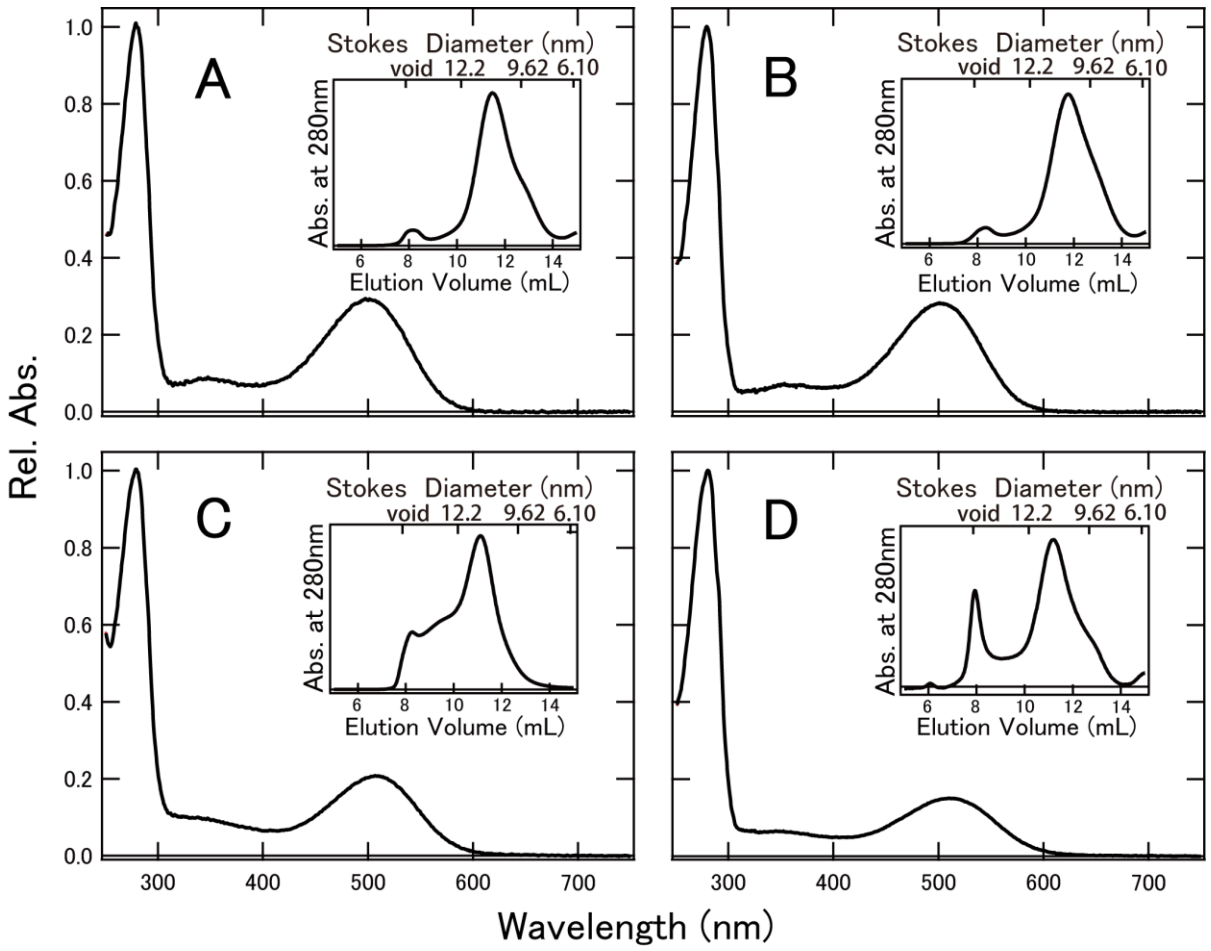
A
B
C
D
Stokes Diameter (nm)
void 12.2 9.62 6.10
Abs. at 280nm
Elution Volume (mL)
Rel. Abs.
Wavelength (nm)

Fig.2

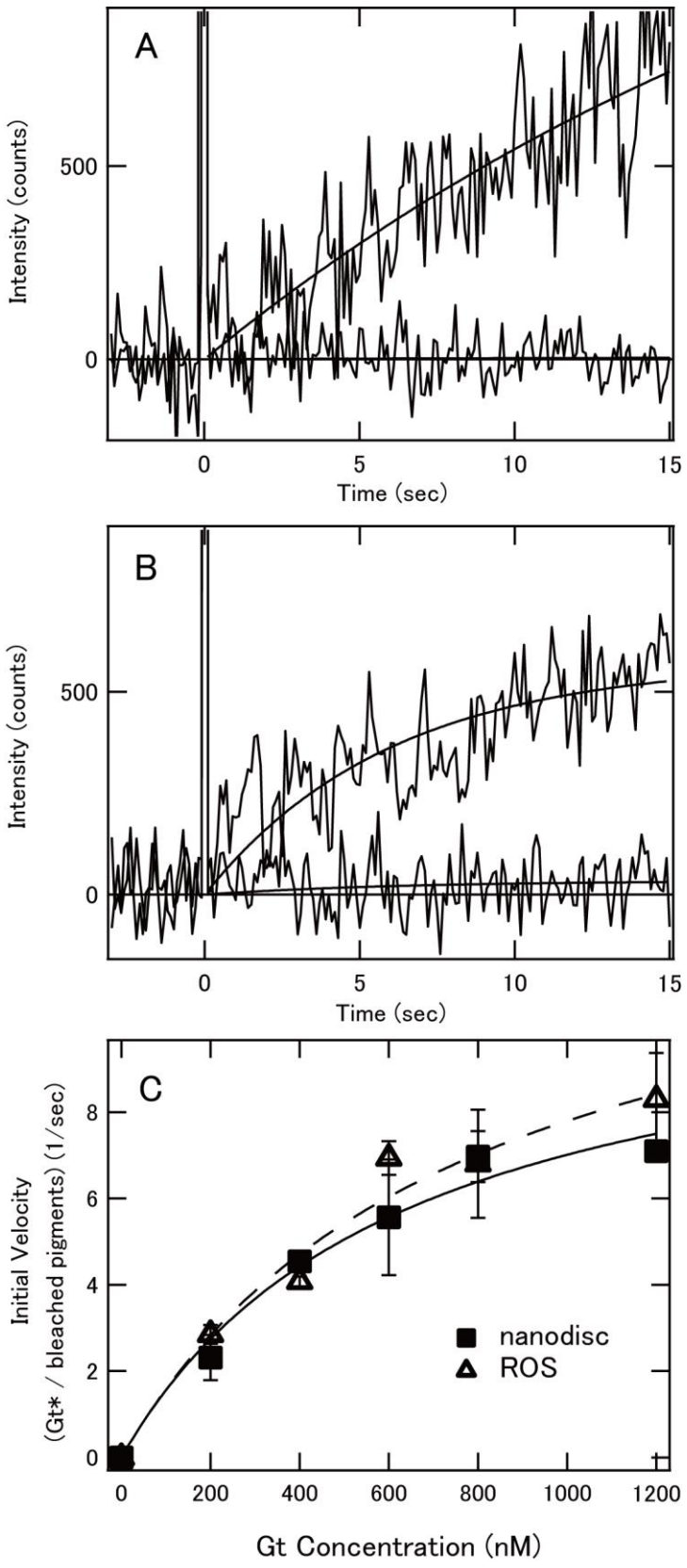
A
Intensity (counts)
500
0
0
5
10
15
Time (sec)
B
Intensity (counts)
500
0
0
5
10
15
Time (sec)
C
Initial Velocity
(Gt* / bleached pigments) (1/sec)
8
6
4
2
0
nanodisc
ROS
0
200
400
600
800
1000
1200
Gt Concentration (nM)

Fig.3

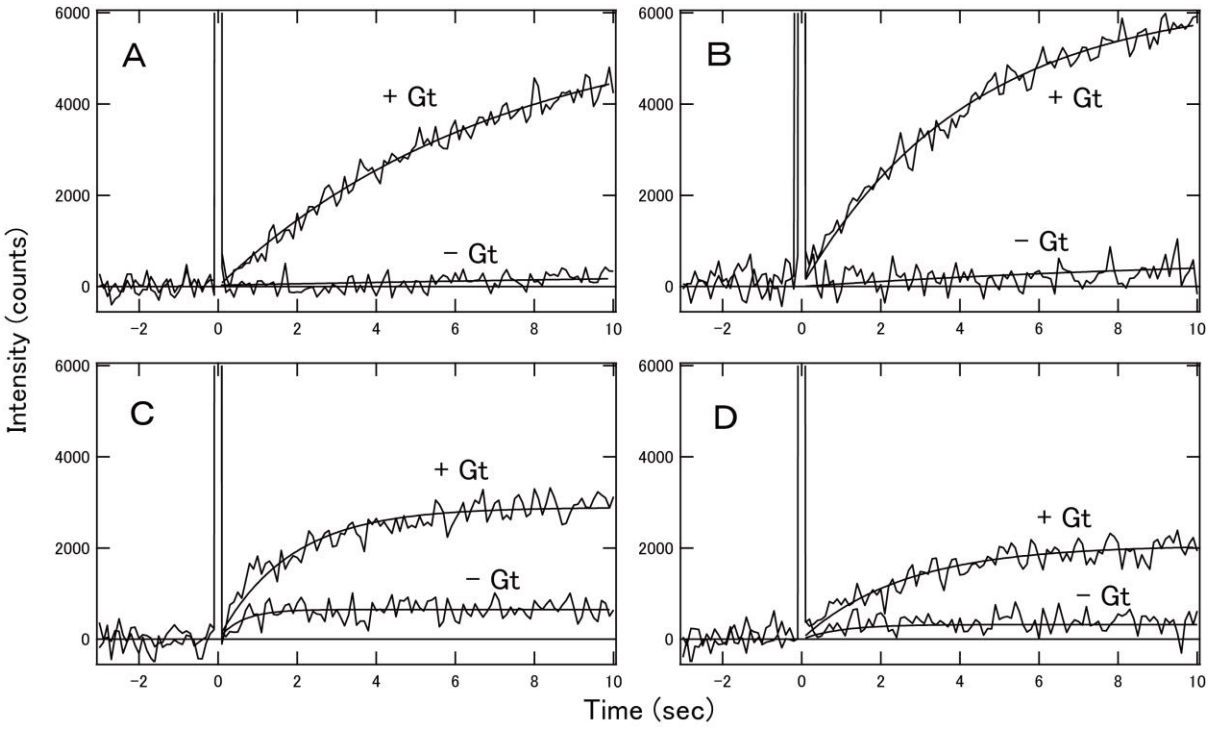
A
B
C
D
+ Gt
− Gt
Intensity (counts)
Time (sec)
6000
4000
2000
0
−2
0
2
4
6
8
10

Fig.4

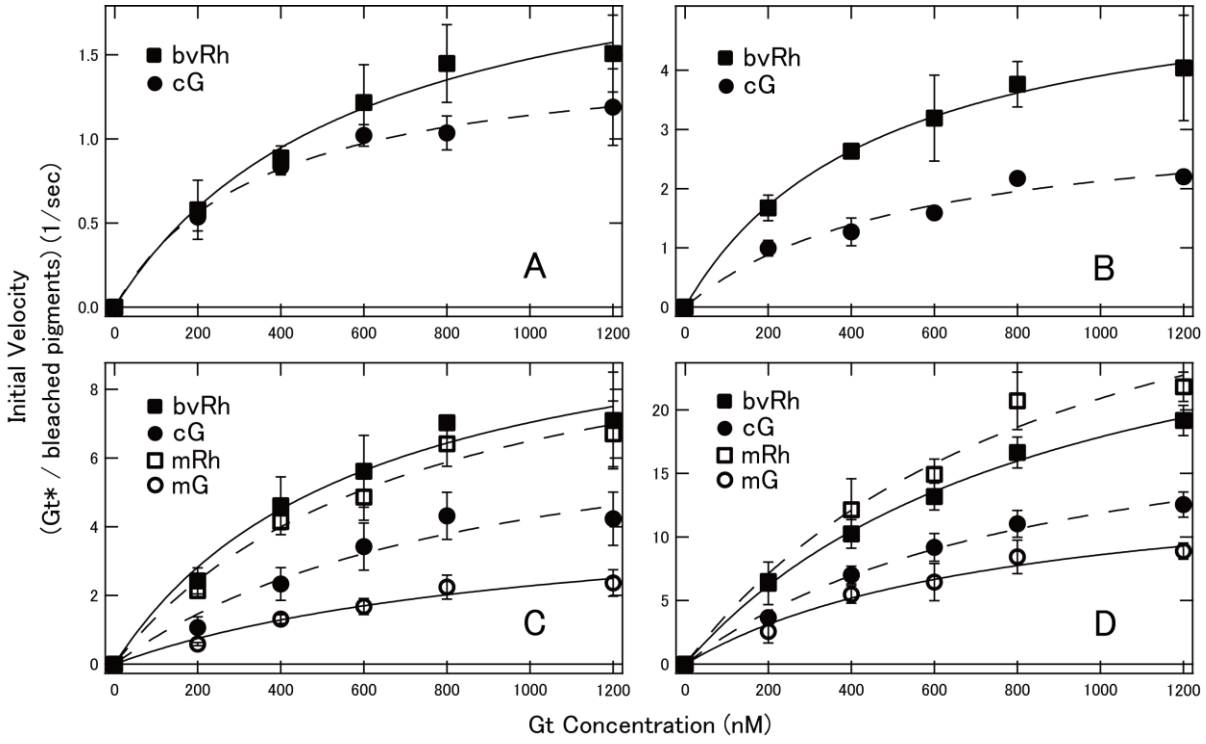
bvRh
cG
mRh
mG
A
B
C
D
Initial Velocity
(Gt* / bleached pigments) (1/sec)
Gt Concentration (nM)

Fig.5

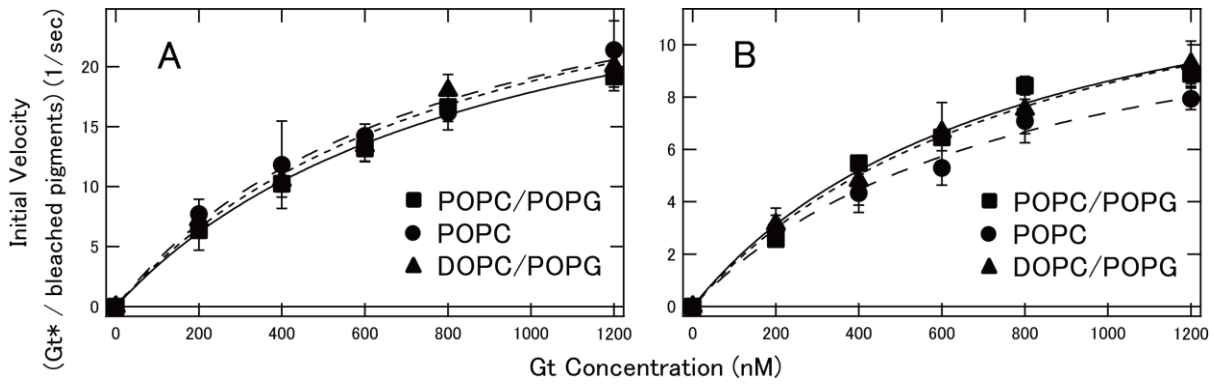
A
B
POPC/POPG
POPC
DOPC/POPG
Initial Velocity
(Gt* / bleached pigments) (1/sec)
Gt Concentration (nM)
0
200
400
600
800
1000
1200
5
10
15
20
2
4
6
8

Fig.6

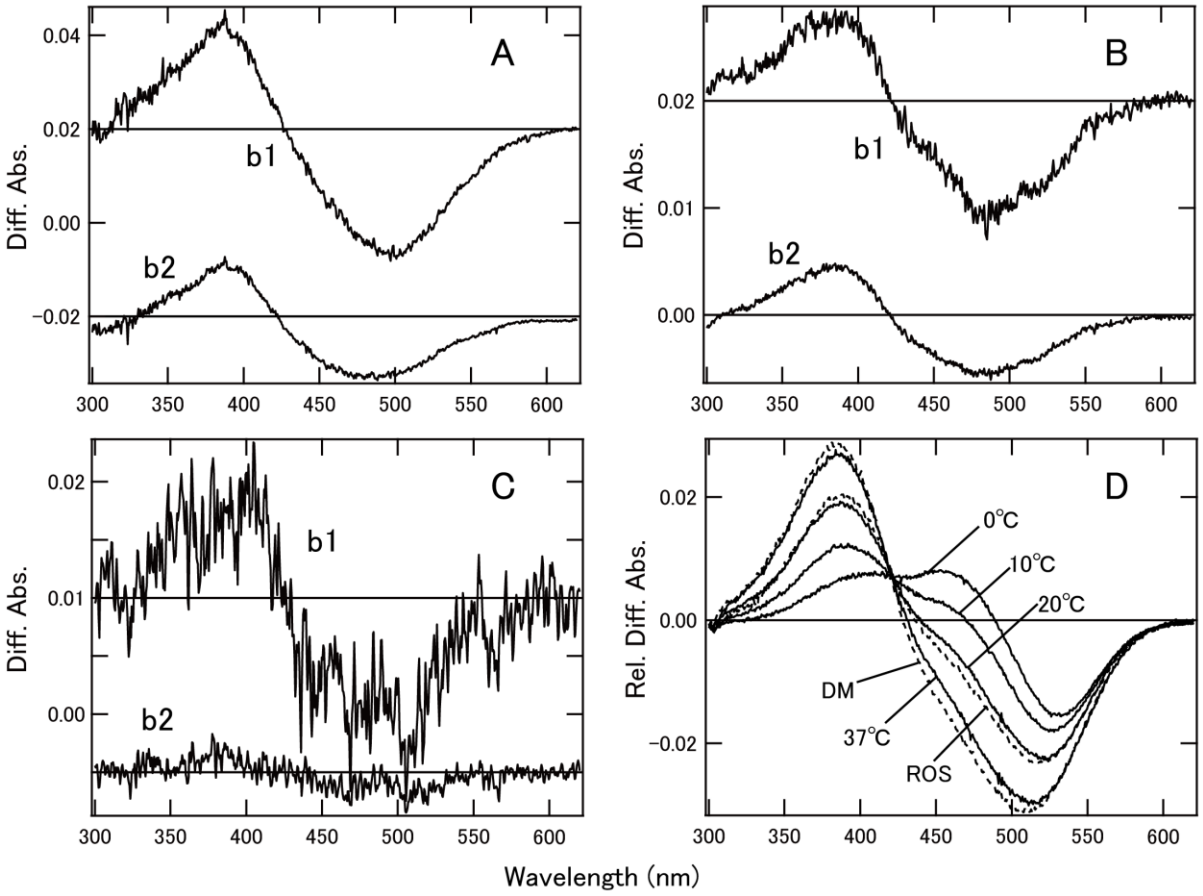
A
B
C
D
b1
b2
Diff. Abs.
Rel. Diff. Abs.
Wavelength (nm)
0°C
10°C
20°C
DM
37°C
ROS

Fig.7

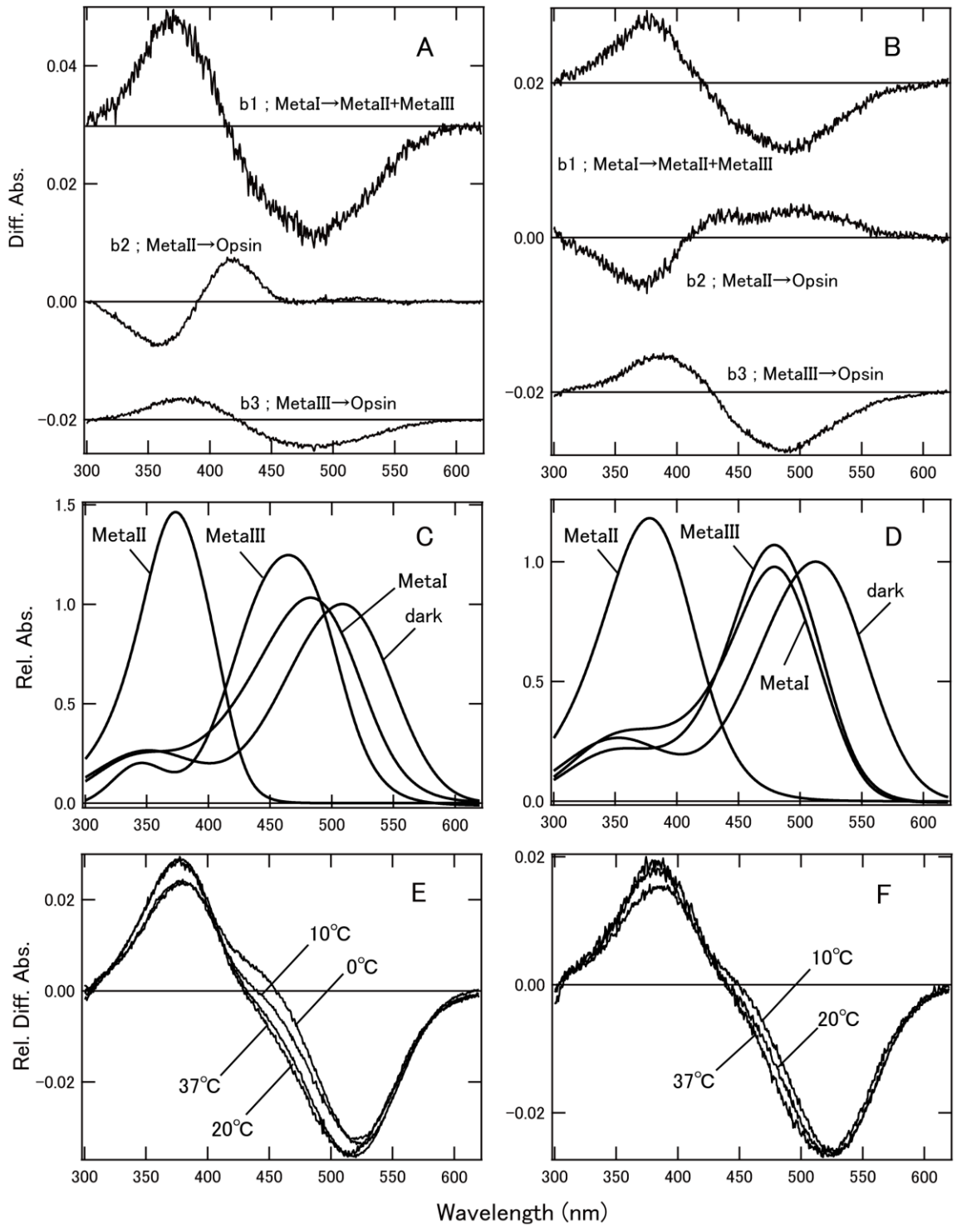
A
b1 ; MetaI→MetaII+MetaIII
b2 ; MetaII→Opsin
b3 ; MetaIII→Opsin
Diff. Abs.
B
b1 ; MetaI→MetaII+MetaIII
b2 ; MetaII→Opsin
b3 ; MetaIII→Opsin
C
MetaII
MetaIII
MetaI
dark
Rel. Abs.
D
MetaII
MetaIII
dark
MetaI
E
10℃
0℃
37℃
20℃
Rel. Diff. Abs.
F
10℃
20℃
37℃
Wavelength (nm)

Fig.8

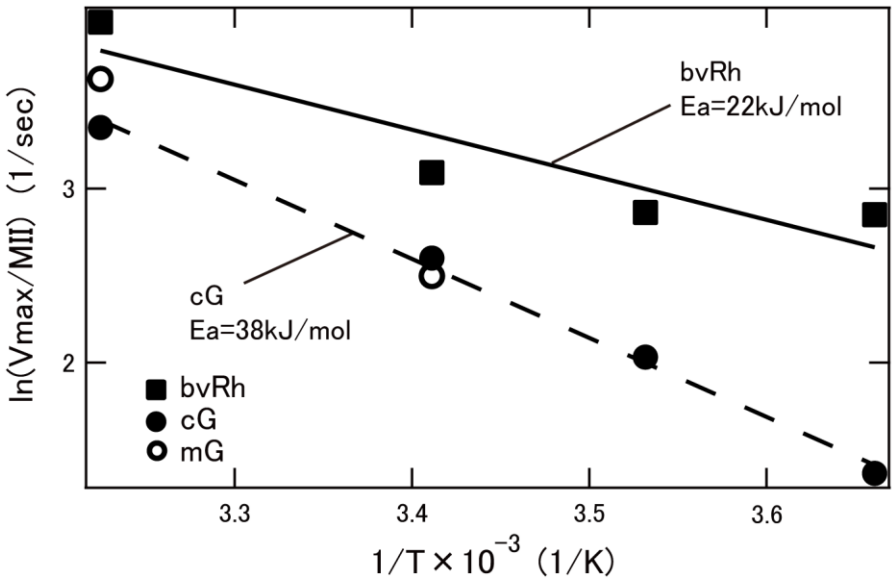
bvRh
Ea=22kJ/mol
cG
Ea=38kJ/mol
bvRh
cG
mG
ln(Vmax/MII) (1/sec)
3
2
3.3
3.4
3.5
3.6
1/T × 10^−3 (1/K)